Density Functional Theory Calculations of Electron Paramagnetic Resonance Parameters of a Nitroxide Spin Label in Tissue Factor and Factor VIIa Protein Complex

Maria Engström

Institute of Physics and Measurement Technology, Linköping University, S-58183 Linköping, Sweden

Juha Vaara

Department of Chemistry, P.O.B. 55 (A.I. Virtasen aukio 1), FIN-00014 University of Helsinki, Finland

Bernd Schimmelpfennig* and Hans Ågren

Department of Biotechnology, Laboratory of Theoretical Chemistry, Royal Institute of Technology, S-10691 Stockholm, Sweden

Received: September 12, 2002

The electron paramagnetic resonance (EPR) **g** and ^{14}N hyperfine coupling (**A**) tensors of a nitroxide spin label are calculated with density-functional theory (DFT). The influence on the spin label from nearby amino acids in the extracellular part of tissue factor (sTF) and activated factor VII (FVIIa) protein complex is investigated. For that purpose, the nitroxide unit and six surrounding amino acids within 5 Å are selected on the basis of a molecular mechanics structure of the protein complex. The effects of the surroundings on the EPR parameters of the spin label can be divided into indirect effects caused by the induced structure changes of the spin label and direct effects. The structural changes are larger in the present case. The experimentally measurable hyperfine tensor component perpendicular to the molecular plane of the spin label, A_{zz}, as well as the **g** tensor component along the NO direction, g_{xx}, are significant probes of the intramolecular structure of the spin label. This indicates the possibility of relating EPR properties to the geometric structure of radical sites. The direct environmental effects on the **g** tensor from the surrounding amino acids mainly affect the second-order spin−orbit/orbital Zeeman cross-term contributions from the spin label itself. The direct effects originating elsewhere in the model are small. Neither the **g** nor **A** tensors display additivity of the effects of individual amino acids on the final observable. The results underline the feasibility of DFT calculations of the EPR parameters in large molecular systems, such as spin labels and other radicals in proteins.

1. Introduction

Structural information on proteins is commonly obtained by X-ray crystallography or nuclear magnetic resonance (NMR) spectroscopy. An alternative technique for proteins that are difficult to analyze with these methods is electron paramagnetic resonance (EPR) spectroscopy combined with site-directed mutagenesis of molecular probes, i.e., spin labels.[1,2] In this technique the spin label is attached to specific protein sites by replacing an amino acid by a cysteine that can be linked to the label. When the label is introduced into the protein, it is influenced by interactions with surrounding structures and the motion of the protein. It is thus possible to monitor molecular interactions and conformational changes in the close vicinity of the label through its EPR spectrum. Site-directed spin labeling and EPR have been applied in folding studies of human carbonic anhydrase II (HCA II),[3,4] for studies of specific protein interactions between HCA II and the chaperonin GroEL,[5] and between the blood coagulation proteins tissue factor (TF) and activated factor VIIa (FVIIa).[6] These studies have focused on the motion of the spin label in different protein environments.

Nitroxide pyrrolidine radicals are commonly used as spin labels in proteins and other macromolecules. These radicals consist of a paramagnetic NO group, a carbon five-ringed structure with methyl groups in the ortho positions that stabilize the radical, and a linker to the protein (Figure 1). The **g** and hyperfine coupling (**A**) tensors of nitroxide spin labels are sensitive to solvent interactions. This has been shown for the isotropic **g** value (g_{iso}) and hyperfine coupling constant (A_{iso}).[7,8] The isotropic values are obtained from EPR at room temperature and constitute rotational averages of the tensor. The anisotropic tensor components can be resolved in frozen solution. It has been shown that the components most sensitive to the polarity of the local environment and to interactions with surrounding molecules, are g_{xx} directed along the NO bond and A_{zz} perpendicular to the plane of the ring structure.[9,10] In particular, hydrogen bonding to the oxygen atom of the nitroxide contributes significantly to g_{iso}, A_{iso}, g_{xx}, and A_{zz} if the radicals are dissolved in protic solvents, such as water or methanol.[7−11] The changes in g_{xx} and A_{zz} are also dependent on the geometric

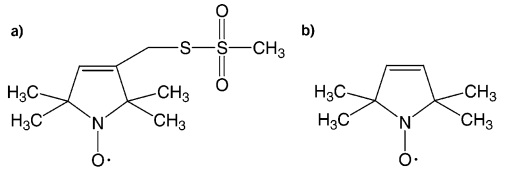

Figure 1. (a) Methanethiosulfonate spin label (MTSSL) and (b) model spin label (MSL) with the cysteine linker removed.

* Corresponding author. E-mail: bernds@TheoChem.kth.se.

10.1021/jp022070t CCC: $22.00
Published on Web 11/05/2002

structure of the nitroxide.[12] From intermediate neglect of differential overlap (INDO) calculations it was found that g_{xx} is sensitive to variations in the geometrical parameters of the NO group but that the effect of remote substituents is relatively small.[13]

Nitroxide spin labels are applicable as probes of local polarity in investigations of membrane proteins. Variations of A_{zz} in rigid-limit EPR spectra on phospholipid bilayers were interpreted to be due to a polarity gradient in the bilayer.[8] A detailed 250 GHz EPR study of the **g** and **A** tensors of spin-labeled lipids yielded lower g_{xx} and higher A_{zz} values when the label was attached near the polar headgroup of the phospholipid membrane instead of in the hydrophobic region.[14] The methanethiosulfonate nitroxide spin label (MTSSL) was recently used as a probe of polarity in studies of the proton channel of the transmembrane proton pump bacteriorhodopsin.[15,16] Nitroxide spin labels are also applicable in structural and functional studies of globular proteins (see, e.g., refs 17 and 18).

A previous paper reported density-functional theory (DFT) calculations combined with 9 and 95 GHz EPR spectroscopy on MTSSL exposed to various types of solvents.[19] Two kinds of solvent effects on the **g** and **A** tensor of MTSSL were considered: (1) electrostatic effects due to the polarity of the solvent, and (2) hydrogen bonding to the oxygen atom. In that study, hydrogen bonding was modeled with water molecules. The effects of a solvent dielectricum on the **A** tensor were also estimated with the polarizable continuum model (PCM).[20] The calculated EPR parameters present the same trends as seen in the experiments. That is, A_{iso} and A_{zz} increase upon hydrogen bonding and in solvents with a high dielectric constant, whereas g_{iso} and g_{xx} decrease. It was also concluded that the effect of a dielectric continuum estimated from the PCM model is only pronounced for low dielectric constants ($\epsilon < 10$). The influence of the hydrogen bonding interaction is much more significant. It is therefore of interest to further explore the specific influence from solvent molecules on the **g** and **A** tensors of nitroxide spin labels.

In the present study we investigate a simplified model of MTSSL, the model spin label (MSL) where the cysteine linker of MTSSL has been removed, in a surrounding protein structure. The complex of two proteins, tissue factor (TF) and factor VIIa (FVIIa), involved in blood coagulation, was chosen for this purpose. When TF comes into contact with the blood after vascular injury, the formation of the TF/FVIIa complex initiates blood coagulation. The crystal structures of both the extracellular part of TF (sTF)[21,22] and of sTF in complex with FVIIa,[23] are known. In a recent study the complex formation between sTF and FVIIa was investigated with site-directed labeling and EPR.[6] A phenylalanine at position 140 (Phe140) was replaced by a cysteine to which the spin label was linked. Phe140 is one of the residues in direct contact with FVIIa in the complex. In that study, molecular mechanics (MM) calculations were performed with the purpose of simulating the structure of MTSSL mutated into sTF complexed with FVIIa. The advantage of MM calculations is the possibility to obtain an estimate of the overall structure of large molecules such as proteins. One of the disadvantages is, however, the inability to treat electronic properties. Here, we use the reasonable MSL model of MTSSL in the sTF/FVIIa complex for DFT calculations of the EPR **g** and **A** tensors. The aim is to investigate, using DFT, the influence on the EPR parameters from the amino acids in the nearest environment of MTSSL in the protein complex. The significance of both the indirect effects occurring through environmentally induced structural changes and the direct electronic effects, are assessed separately.

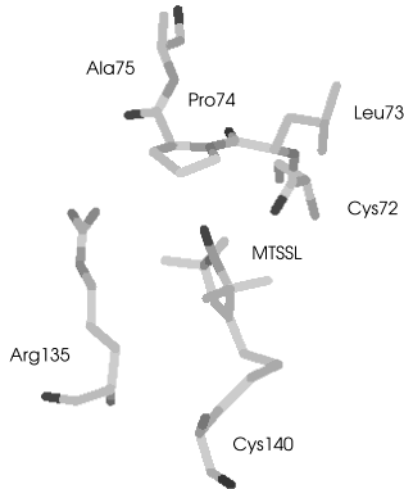

Figure 2. MTSSL with amino acids within 5 Å in the sTF/FVIIa protein complex.

2. Methods

Partial DFT geometry optimizations were performed using the Becke−Lee−Yang−Parr (BLYP)[24,25] exchange-correlation functional and starting from the energetically most favorable MM structure of MTSSL in the sTF/ FVIIa complex[6] (Figure 2). The protein environment was modeled with all amino acids within 5 Å from the spin label in the MM structure, i.e., Arg135 and Cys140 of sTF, as well as Cys72, Leu73, and Pro74 of FVIIa (Figure 2). Ala75 was included in the model to prevent an inconsistent spin density accumulation on Pro74. In these calculations, the NO distance and the C_1-NO-C_5 dihedral angle of the label were optimized whereas all other geometrical parameters were kept fixed. The 6-31G** basis set was used on the nitrogen, oxygen, and carbon atoms of the nitroxide and the D95[26] basis set on all remaining atoms. The spin multiplicity was set to 2 and the charge to +1 because arginine contains charged groups. The geometry optimizations were carried out with the Gaussian 98 program package.[27]

The EPR parameters of MSL, MTSSL, and MSL in the protein environment were calculated with the Becke−Perdew86 (BP86)[24,28] and Perdew86 (P86)[28,29] exchange-correlation functionals in the deMon Kohn−Sham program[30−32] linked with a local version of the deMon−NMR−EPR property code.[33] In the course of this work it became apparent that the computationally attractive locally dense basis set concept, devised for NMR nuclear shieldings by Chesnut et al.,[36,37] is not easily applicable for the environmental effects on the **g** tensor, which is a more global property than the NMR parameters. Hence, the IGLO-II basis set, based on the original work of Huzinaga[34] as well as moderately contracted and supplemented with polarization functions by Kutzelnigg et al.,[35] was used uniformly for all the atoms. The effect of basis set truncation was estimated by repeating the calculations for MSL, MTSSL, and models containing MSL and one of the surrounding amino acids at a time, with the more flexible IGLO-III set[34,35] used for all atoms. The (5,4;5,4) auxiliary basis was chosen for sulfur atoms, (5,2;5,2) for carbon, nitrogen, and oxygen atoms, and (5,1;5,1) for hydrogens. In this notation, the first two digits denote the number of s-primitives and spd shells (sharing a common exponent) for fitting the electron density. The two remaining numbers denote the same for the exchange-correlation potential.

The FINE angular integration grid of deMon was used with 32 points of radial quadrature.[31,32] To improve the quality of the Kohn−Sham molecular orbitals used in the property calculation, a compromise strategy[30] was applied in which an extra iteration, with a larger grid and without the fit of the exchange-correlation potential, was added after the initial convergence had been reached.

A routine for **g** tensor calculations was recently developed and incorporated into deMon−NMR−EPR[33] and subsequently applied for *p*-semiquinone radicals[38] and tryptophan−quinone complexes.[39] The method is based on the Breit−Pauli level Hamiltonian and contains all terms up to the second order in the fine structure constant α, except the two-electron gauge correction that is estimated to be of minor importance.[40] The included contributions are the first-order relativistic mass correction (RMC) and one-electron gauge correction (GC), as well as the second-order orbital Zeeman/electronic spin−orbit (SO/OZ) terms. We refer to ref 33 for further details.

In the **g** tensor calculations, the gauge origin problem was tackled with the individual gauge for localized orbitals (IGLO) method[35] using the Pipek−Mezey (PM)[41] algorithm for localizing the orbitals. The orbitals corresponding to the 1*s* orbitals of the first-row atoms as well as the 1s2s2p orbitals of S were localized separately from all the valence orbitals. The full one- and two-electron spin−orbit operator was approximated by an effective one-electron/one-center operator[42] using the AMFI software.[43] This has been demonstrated to provide very accurate reproduction of the results of the full operator[33] but avoids the explicit calculation of all multi-center integrals as well as the storage of two-electron spin−orbit integrals. It therefore allows calculations on large systems without significant loss of accuracy. It is noteworthy that this approach includes exchange-type spin−orbit terms as well as the so-called spin-other-orbit terms originating from the Breit interaction.[44]

The noniterative sum-over-states (SOS) approach for the SO/OZ term[30,33] makes it simple and computationally efficient to include the coupling to the excited states, because only the Kohn−Sham orbital energies and matrix elements between the ground state and singly excited determinants have to be calculated. Most of the present calculations have used the uncoupled DFT approach[45] resulting from pure (nonhybrid) DFT functionals of the electron density alone. We test our final **g** tensor results also against the influence of the "Malkin correction" of the orbital energy denominators in the second-order term, in the sum-over-states density-functional perturbation theory (SOS-DFPT) approach.[45] We refer to the original paper for details. For calculating the **A** tensor, we have used the deMon-EPR property routines that have been available for a few years.[30,46] They include the nonrelativistic first-order terms, i.e., the expectation values of the Fermi contact and spin−dipole hyperfine operators that give rise to isotropic and anisotropic contributions to the hyperfine coupling tensor, respectively.

3. Results and Discussion

3.1. Geometric Structure. Earlier experimental[12] and computational[13] studies have shown that the EPR parameters are dependent on the geometric structure of the nitroxide radical. An examination of the structural parameters obtained from the MM calculation of MTSSL in the sTF/FVIIa complex[6] reveals that the NO bond length is ca. 0.2 Å longer as compared to the DFT calculations. The MM bond length is R(NO) = 1.48 Å, whereas the BLYP distance equals R(NO) = 1.29 Å in the protein model (Figure 2). Earlier B3LYP results yielded R(NO) = 1.28 Å at full optimization of MTSSL.[47] Calculations predict a planar structure of the ring moiety in MSL. The C_1-NO-C_5 dihedral angle of MTSSL does not correspond to a planar configuration in either the MM or DFT calculations of the complex. However, the out-of-plane distortion is smaller in the DFT optimization (185°) than in the MM structure (191°). The distance between the ring carbons and the nitrogen is slightly shorter (by ca. 0.03 Å) in the MM structure as compared to the DFT structure.

TABLE 1: Calculated EPR Parameters for the Free Model Spin Label (MSL) with Different Structural Parameters[a]

property	B3LYP[b]	R(NO) = 1.48 Å[c]	R(CN) = 1.47 Å[c]	C_1-NO-C_5 = 200°[d]
g_{xx}	6055	8672	6192	6278
g_{yy}	3417	4030	3399	3374
g_{zz}	−172	−226	−165	−189
A_{iso}	7.20	7.66	6.85	10.11
$A_{dip,zz}$	18.13	17.95	17.97	17.58

[a] Calculations using the Perdew86 functional and IGLO-II basis at B3LYP/6-31G** optimized geometry for MSL, apart from the indicated structural parameters. The **g** tensor shift from the free-electron value is indicated in ppm, and the hyperfine coupling values to ^{14}N are given in Gauss. $A_{zz} = A_{iso} + A_{dip,zz}$. [b] Reference structure; R(NO) = 1.28 Å, R(CN) = 1.50 Å, and C_1-NO-C_5 planar. [c] Molecular mechanics value for the MTSSL in protein complex. [d] 200° is representative of the off-plane distortions.

As the **g** and **A** tensors are sensitive to the geometrical parameters of the NO group, it is of importance to make a systematic investigation of the structural dependence. For that purpose, the NO and CN bond lengths as well as the C_1-NO-C_5 dihedral angle of MSL were varied between extreme values, enclosing both the MM and DFT structures. The reference structure is that of the B3LYP-optimized free MSL. Table 1 displays the results, calculated using the P86 functional.

It is seen that the **g** tensor component, g_{xx}, along the NO bond increases substantially with increasing NO bond length. The g_{xx} value from the MM structure of MSL is 2620 ppm (parts per million) larger than the corresponding value from the DFT structure. Also the *y* component increases substantially at longer NO bond lengths, $g_{yy}(MM) - g_{yy}(DFT) = 610$ ppm. The out-of-plane component g_{zz} remains approximately constant in the calculated interval. A_{iso} increases by 0.46 G, whereas minor changes for the dipolar terms are observed.

The isotropic **A** value of MSL is extremely sensitive to the C_1-NO-C_5 dihedral angle. $A_{iso} = 10.11$ G in a structure with the angle of 200°, whereas the value for the planar structure is 2.9 G lower. The anisotropic dipolar component, $A_{dip,zz}$ is 0.6 G lower in the 200° structure and the changes in the *x* and *y* components are less pronounced. g_{xx} is slightly dependent on the C_1-NO-C_5 angle. The difference between the planar structure and a structure with the angle equal to 200° is 220 ppm, with the higher g_{xx} value obtained for the 200° structure. Small changes are observed for different CN distances. In summary, g_{xx} and g_{yy} that increase at larger bond lengths, as well as A_{iso} that increases with increasing dihedral angle, are the EPR parameters most sensitive to the geometric structure of the free model spin label.

3.2. Protein Environment. *3.2.1. General Information.* MTSSL is enclosed in a pocket inside the protein complex. Cys72, Leu73, Pro74, and Ala75 of FVIIa form a semicircle around the NO group of the nitroxide spin label. Cys72 is closest to the radical with a distance between the nitroxide and carboxyl oxygens *R*(OO) = 2.66 Å. Leu73 and Pro74 are more remote with O−O distances of 3.94 and 5.43 Å, respectively. The distance between the nitroxide and Ala75 oxygens is 8.48 Å.

The spin density for a free nitroxide radical is located at the nitrogen and oxygen atoms to almost equal extent.[47] The spin

TABLE 2: Calculated Isotropic and Anisotropic Values of the g Tensor for the MTSSL Spin Label, Its Reduced Model MSL, and MSL in the Presence of Various Amino Acids in the sTF/FVIIa Protein Complex (Figure 2)[a]

molecular model[b]	basis	g_{iso}	g_{xx}	g_{yy}	g_{zz}
MSL	IGLO-II	3092	6177	3299	−199
	IGLO-III	3150	6395	3256	−201
MTSSL	IGLO-II	3086	6157	3305	−203
	IGLO-III	3137	6375	3241	−207
MSL + Cys	IGLO-II	3053	6101	3283	−225
	IGLO-III	3116	6302	3271	−227
MSL + Leu	IGLO-II	3089	6152	3311	−197
	IGLO-III	3166	6354	3341	−198
MSL + Pro	IGLO-II	3082	6121	3320	−194
	IGLO-III	3145	6346	3282	−193
MSL + Ala	IGLO-II	3098	6183	3311	−200
	IGLO-III	3143	6378	3251	−201
MSL + Arg	IGLO-II	3057	6102	3267	−197
	IGLO-III	3112	6299	3235	−199
MSL + Cys + Leu	IGLO-II	3046	6008	3327	−198
MSL + Pro + Ala	IGLO-II	3081	6118	3319	−193
MSL + Cys + Leu + Pro	IGLO-II	3014	5941	3302	−202
MSL + Cys + Leu + Pro + Ala	IGLO-II	3013	5940	3302	−203
MSL + Cys + Leu + Pro + Ala + Arg	IGLO-II	2996	5895	3288	−195
	extrap[c]	3050	6100	3260	−200
exp[6]		3080(50)	5700	3600	0

[a] The Becke−Perdew functional was used. Results in ppm. The structure is partially geometry optimized for the largest MSL + Cys + Leu + Pro + Ala + Arg system. The partial optimization was done at the BLYP/6-31G** level, covering the NO distance and C_1-NO-C_5 angle of the spin label. [b] MSL is the pyrrolidine nitroxide radical without linker, MTSSL is the spin label linked to Cys140, Cys = cysteine 72, Leu = leucine 73, Pro = proline 74, Arg = arginine 135, and Ala = alanine 75. [c] Extrapolated value based on the calculated result for the MSL + Cys + Leu + Pro + Ala + Arg system obtained with the IGLO-II basis set, to which the average changes from the IGLO-II to the IGLO-III results for the small systems are added.

TABLE 3: Calculated Isotropic and Anisotropic Values of the A Tensor for the MTSSL Spin Label, Its Reduced Model MSL, and MSL in the Presence of Various Amino Acids in the sTF/FVIIa Protein Complex (Figure 2)[a]

molecular model	basis	A_{iso}	$A_{dip,zz}$
MSL	IGLO-II	7.65	17.98
	IGLO-III	7.88	18.63
MTSSL	IGLO-II	7.67	17.98
	IGLO-III	7.90	18.63
MSL + Cys	IGLO-II	7.85	18.09
	IGLO-III	8.02	18.68
MSL + Leu	IGLO-II	7.69	18.13
	IGLO-III	7.91	18.73
MSL + Pro	IGLO-II	7.73	18.05
	IGLO-III	7.93	18.66
MSL + Ala	IGLO-II	7.69	18.05
	IGLO-III	7.91	18.68
MSL + Arg	IGLO-II	8.12	18.34
	IGLO-III	8.33	18.97
MSL + Cys + Leu	IGLO-II	7.90	18.20
MSL + Pro + Ala	IGLO-II	7.75	18.11
MSL + Cys + Leu + Pro	IGLO-II	8.17	18.46
MSL + Cys + Leu + Pro + Ala	IGLO-II	8.18	18.47
MSL + Cys + Leu + Pro + Ala + Arg	IGLO-II	8.59	18.69
	extrap[b]	8.8	19.3
exp[6]		15.9	18.8

[a] The Perdew86 functional was used. Otherwise see footnotes to Table 2. The hyperfine coupling values to ^{14}N are given in Gauss. $A_{zz} = A_{iso} + A_{dip,zz}$ corresponds to the experimental anisotropic value. [b] Extrapolated value based on the calculated result for the MSL + Cys + Leu + Pro + Ala + Arg system obtained with the IGLO-II basis set, to which the average changes from the IGLO-II to the IGLO-III results for the small systems are added.

density distribution for MTSSL as obtained with the BLYP method is $\rho_N = 0.43$ and $\rho_O = 0.50$. The main part of the spin density remains located at the NO group of the nitroxide also in the protein model; $\rho_N = 0.47$ and $\rho_O = 0.46$. The total spin density on the NO group is equal in the two models ($\rho = 0.93$) but transfer occurs from oxygen to nitrogen in the protein model.

The calculated **g** and **A** tensors for MSL, MTSSL, and the different models for the protein environment are displayed in Tables 2 and 3. Cys140 of TF, which constitutes the linker of the label to the protein, is seen not to affect the EPR parameters appreciably. The difference in g_{iso} and A_{iso} between the minimal model without linker (MSL) and MTSSL is less than the experimental errors, ±50 ppm and ±0.5 G for g_{iso} and A_{iso}, respectively. This result is consistent with the retained spin density distribution in the different models of the label.

*3.2.2. **g** Tensor.* In all models, the component g_{zz} orthogonal to the plane defined by the nitroxide and the connected five-ring is almost independent of the surrounding molecules. However, the **g** tensor component along the NO bond, g_{xx}, and the perpendicular component, g_{yy}, show large variations depending on which amino acids occur in the model (Table 2). The general trend is that these values are lower in models including amino acids as compared to the free spin label.

Among the amino acids within 5 Å in the selected protein model, Cys72 and Arg135 cause the largest changes to the **g** tensor. This is somewhat expected, as these amino acids are close to the spin label, roughly on the opposite sides along the normal of the plane of the label. We note in passing that for a locally dense basis set, where the environment of the spin label is described only at the valence double-ζ level, the relatively distant Pro74 amino acid was found to cause much larger effects than the two close-by amino acids. The present results, obtained at a uniform basis set level are qualitatively different. Both Cys72 and Arg135 cause changes of roughly −40 to −35 and −95 to −75 ppm (slightly depending on the basis set used) on g_{iso} and g_{xx}, respectively. The effect of Pro74 on the same tensor component, in the *x* direction from the spin label, is roughly −50 ppm, but there is hardly any effect on g_{iso} due to compensating changes of the other principal components of the **g** tensor.

Leu73 is bonded to Cys72 in the structure, and adding the former first to MSL and then to MSL + Cys models displays a nonadditivity of the g_{xx} tensor component. In MSL + Cys + Leu, g_{xx} is 169 ppm below the value of MSL, whereas only −100 ppm would be expected assuming additivity of the effects of the two amino acids. Enlarging the model with the next amino acid, Pro74, reveals nonadditivity of the g_{yy} component in the plane of the label but perpendicular to the line joining the spin label with the five-ring of Pro. g_{yy} increases by 20−30 ppm from MSL to MSL + Pro, to be compared with the 25 ppm *decrease* from MSL + Cys + Leu to MSL + Cys + Leu + Pro. The effects of adding the distant Ala75 amino acid to the plain MSL, MSL + Pro, or MSL + Cys + Leu + Pro models are small, and this amino acid is unimportant in the present modeling of the **g** tensor. Apart from the Pro effect on g_{yy}, the combined effects caused by the two subunits (Cys72 + Leu73) and (Pro74 + Ala75) are fairly additive. The nonadditivity continues when the important, positively charged, Arg135 amino acid is finally added. Its effect is reduced in the MSL + Cys + Leu + Pro + Ala + Arg model as compared to MSL + Arg. Although Arg135 is not directly bonded to the rest of the model, one of the NH_2 groups of Arg135 is close to the carbonyl oxygen of Pro74 (OH distance 2.9 Å). Overall, the nonadditivity of the effects of individual amino acids points to a sensitivity of the results to the details of model construction.

Comparison of the IGLO-II and IGLO-III results gives information about the basis set convergence for MSL, MTSSL,

TABLE 4: Calculated Physical Contributions to the DFT g Tensor[a]

property	term[b]	MSL	MTSSL	MSL + Cys + Leu + Pro + Ala + Arg
g_{iso}	RMC	−291	−291	−291
	GC	142	143	134
	SO(1)/OZ	5098	5090	4970
	SO(2)/OZ	−1856	−1855	−1818
g_{xx}	GC	179	179	166
	SO(1)/OZ	9874	9847	9468
	SO(2)/OZ	−3585	−3578	−3449
g_{yy}	GC	166	166	152
	SO(1)/OZ	5385	5393	5408
	SO(2)/OZ	−1960	−1963	−1981
g_{zz}	GC	81	82	84
	SO(1)/OZ	35	30	34
	SO(2)/OZ	−24	−23	−23

[a] All calculations with the BP86 exchange-correlation functional and IGLO-II basis. Otherwise see footnotes to Table 2. [b] Physical contributions as follows:[33] relativistic mass correction (RMC), one-electron gauge correction (GC), one-electron spin−orbit/orbital Zeeman second-order term [SO(1)/OZ], and the corresponding two-electron term [SO(2)/OZ]. The SO(1)/OZ term is obtained using a one-center approximation for the 1-electron SO operator, and the SO(2)/OZ term as the difference of the full AMFI operator and SO(1)/OZ. The RMC term is isotropic.

and models containing MSL and one amino acid at a time. The larger basis is seen to rather systematically increase g_{xx} by 200 ppm, whereas g_{yy} is decreased but much less, leading to a roughly 60 ppm net increase in g_{iso}. The systematic changes allow basis set effects to be extrapolated also for the larger systems, for which explicit IGLO-III calculations would be very expensive, see section 3.2.4 below.

Table 4 lists the **g** tensor contributions for MSL, MTSSL, and the largest of the present models, arising from the different physical mechanisms: RMC, GC, as well as the SO/OZ term featuring both the one- [SO(1)/OZ] and two-electron [SO(2)/OZ] spin−orbit interaction. The data for MSL and MTSSL are practically the same, underlining the detailed equivalence of these two systems. The protein environment in the MSL + Cys + Leu + Pro + Ala + Arg model is seen to mainly affect the second-order SO/OZ terms, decreasing the one-electron contribution to g_{xx} by 410 ppm and the magnitude of the corresponding, negative two-electron term by 140 ppm. The other changes are small, leaving the change of the total SO/OZ contribution to g_{iso} due to the protein environment at −90 ppm.

As the effective AMFI spin−orbit operators arise from atomically additive contributions (also for the two-electron terms), an atomic decomposition of the spatial origin of the second-order term can be carried out. The data for Δg_{iso} is shown in Table 5. Over 80% of the total **g** shift arises due to the spin−orbit interaction at the oxygen atom in the free MSL. The remaining shift is then due to the nitrogen of the NO group. This picture is practically identical in MTSSL, particularly the direct effect of the Cys140 linker is seen to be negligible. In the largest protein model, the direct environmental effects on the **g** shift of MSL are of dual character. First, the contribution of the atoms belonging to the surrounding amino acids is only about 40 ppm. Overall, the transfer of spin density from the spin label to the protein environment is of experimentally negligible magnitude. More important are the changes induced on the spin label by the environment, visible as a 160 ppm decrease of the contribution of the oxygen atom of the NO group. At the same time, the contribution of N increases by 20 ppm. This behavior parallels that observed for the spin density distribution in the nitroxide group, discussed above.

TABLE 5: Breakdown of the Calculated Second-Order Contribution to the Isotropic g Factor into Contributions from Various Regions of the Molecular Model[a]

atom/fragment	MSL	MTSSL	MSL + Cys + Leu + Pro + Ala + Arg
N	531	533	555
O	2699	2695	2536
ring CH	−3	−3	1
methyl groups	15	12	19
cys linker		−3	
total spin label	3242	3235	3111
environment			41
Σ[b]	3242	3235	3153

[a] The SO(1+2)/OZ contribution to g_{iso} in the AMFI approximation. The BP86 exchange-correlation functional and IGLO-II basis, were used. Otherwise see footnotes to Table 2. Results in ppm. [b] Sum of the contributions from the spin label and environment.

*3.2.3. **A** Tensor.* Direct effects due to the presence of the different models of the protein environment are observed for the isotropic and dipolar parts of the **A** tensor (Table 3). It is seen that the **A** tensor is larger in the amino acid-containing models compared to the free spin label.

Regarding the changes due to individual amino acids, Cys72 and Arg135 cause changes of the experimentally measured anisotropic quantity, $A_{zz} = A_{iso} + A_{dip,zz}$, from 0.2 to 0.3 and 0.8 G, respectively, as compared to the MSL value. The latter change is larger than the experimental error. The effect of Cys72 is also nonnegligible. The most important amino acids in the protein model are hence seen to be the same for the **A** tensor as for the **g** tensor. Increasing the size of the molecular model increases the differences with respect to the MSL values. The effect is prominent on A_{zz}, because both the isotropic and dipolar parts contribute in the same direction. The relatively low sensitivity of the **A** tensor to specific interactions from the different amino acids should be compared to the high sensitivity to the dihedral C_1-NO-C_5 angle.

Similarly as in the **g** tensor case, the additivity of the environmental effects due to the individual amino acids can be assessed on the basis of the results for the different models. Additivity is seen to be roughly obeyed within the (Cys72 + Leu73) and (Pro74 + Ala75) subunits, but a strong deviation is observed when adding Pro74 to the MSL + Cys + Leu system. The effect of Arg135 seems to, in turn, be relatively independent of the presence of other amino acids in the model. This behavior is the opposite to the effect of the addition of Arg135 on the **g** tensor.

The change from IGLO-II to the larger IGLO-III leads to very systematic changes in A_{iso} and $A_{dip,zz}$ of 0.2 and 0.6 G, respectively, regardless of the details of the model.

In the earlier study[19] it was concluded that polar environment and hydrogen bonding to nitroxide spin labels cause increased **A** values and decreased **g** values. In the present study, a large molecular model is used to mimic a *nonpolar* environment of a spin label inside a protein. In Tables 2 and 3 it is shown that the **g** values decrease and **A** values increase with respect to the MSL values also in the nonpolar molecular model. This explains why the former calculations exaggerated the influence of hydrogen bonding as compared to experimental results.

3.2.4. Comparison with Experimental Data. Experimental measurements of MTSSL in sTF/FVIIa were performed with X-band EPR at room temperature by Owenius et al.[6] In that study, the obtained experimental isotropic **g** value was $g_{iso} = 2.00540 \pm 0.00005$ and the **g** tensor components used in simulations of the EPR spectrum were $g_{xx} = 2.0080$, $g_{yy} = 2.0059$, and $g_{zz} = 2.0023$. The simulation values serve as

TABLE 6: Dependence of the Calculated g and A Tensors on the DFT Exchange Correlation Functional Used[a]

property	functional	MSL	MTSSL	MSL + Cys + Leu + Pro + Ala + Arg	exp[6]
g_{iso}	P86	3101	3095	3004	
	BP86	3092	3086	2996	
	BP86 + Loc.1	2879	2871	2903	3080(50)
g_{xx}	P86	6181	6163	5894	
	BP86	6177	6157	5895	
	BP86 + Loc.1	5577	5585	5639	5700
g_{yy}	P86	3310	3314	3307	
	BP86	3299	3305	3288	
	BP86 + Loc.1	3259	3228	3266	3600
g_{zz}	P86	−190	−193	−187	
	BP86	−199	−203	−195	
	BP86 + Loc.1	−199	−200	−195	0
A_{iso}	P86	7.65	7.67	8.59	
	BP86	5.83	5.86	6.68	15.9
$A_{dip,zz}$	P86	17.98	17.98	18.69	
	BP86	17.88	17.89	18.53	18.8

[a] Comparison between Perdew86 (P86) and Becke−Perdew (BP86) functionals. For **g** tensors, also the BP86 results with the "Malkin correction" of the orbital energy denominators (BP86 + Loc.1), are reported. IGLO-II basis set used throughout.

guidance for the approximate magnitude of the tensor components. A more detailed investigation with high field EPR is required to properly resolve the **g** tensor components.

The calculated **g** tensor for the largest model, MSL + Cys + Leu + Pro + Ala + Arg, is in qualitative agreement with experiment. Though g_{xx} is somewhat overestimated, g_{yy}, g_{zz}, and g_{iso} are below the experimental value, in the last case outside the error limits. Due to the systematic behavior upon improving the basis set, we may extrapolate the effect of using the IGLO-III basis in the MSL + Cys + Leu + Pro + Ala + Arg model. The result of this extrapolation is indicated in Table 2. Although this procedure enhances the agreement of g_{iso} with experiment, this happens at the cost of increasing g_{xx} and decreasing g_{yy} further away from the experimental results. Hence, improvement of the calculated **g** tensor should most likely not be sought from further basis set effects.

To test the effect of the choice of the exchange-correlation functional on the comparison with experiment, Table 6 compares calculations with the P86 and BP86 functionals, as well as BP86 with the Malkin correction (BP86 + Loc.1). Not only is g_{zz} insensitive as always, but also the results for g_{xx} and g_{yy}, and consequently g_{iso}, depend only slightly on the P86/BP86 choice. A larger effect is seen to result from the use of the Malkin correction that decreases particularly the g_{xx} component significantly, bringing it into a closer agreement with experiment. The comparison with the most reliable experimental number, g_{iso}, is made worse by Loc.1, however. Hence, no clear preference among the three DFT methods is borne out from the comparison. We conclude that BP86, for which most of the present data are reported, is representative of the performance of pure DFT functionals for the present organic, light main-group system.

The experimental X-band EPR values of the **A** tensor are $A_{iso} = 15.9$ G and $A_{zz} = 34.7$ G.[6] Although increasing the model size and the basis set size (with extrapolation for the largest model as discussed above for the **g** tensor) improves the agreement with experiment, the calculated results for A_{iso} remain much smaller than the experimental value. The behavior is typical for pure DFT functionals in π-radicals,[48] where A_{iso} is due to spin polarization of other molecular orbitals than the singly occupied orbital (SOMO). In contrast to the relatively accurately calculated direct SOMO contribution of σ-type radicals, spin polarization is much harder to describe quantitatively by using DFT.[49] Hybrid functionals would most likely perform better in comparison with the experiment.[50] The calculated absolute dipolar components are, however, in good agreement with the experiment. The P86 functional is seen to perform better than BP86.

4. Conclusions

The prospects of using nitroxide spin labels as sensors of local protein environment rely on the possibility of obtaining detailed information about the solvent dependence of the EPR parameters. In the present study, we investigate the interaction between the nitroxide spin label MTSSL and nearby amino acids in the sTF/FVIIa protein complex. The minimal model for the spin label (MSL) was used in the calculations of EPR parameters in the protein environment, as neither the spin density distribution nor the EPR parameters changed significantly upon expanding the model from MSL to MTSSL linked with Cys140.

In the case of the **g** tensor, the total environmental influence can be classified into three contributions of decreasing importance: (1) There are changes in the geometry of the spin label, particularly the NO bond length. The component g_{xx} along the NO bond, as well as g_{yy} in the molecular plane of the spin label, increase with increasing R(NO). (2) The second-order **g** tensor contribution (the cross-term between the spin−orbit coupling and the orbital Zeeman interaction) of the spin label itself is modified. (3) There is a practically negligible direct contribution of the surrounding protein environment of the spin label. Similarly, the isotropic hyperfine coupling constant is also most sensitive to the intramolecular structure of the spin label, the C_1-NO-C_5 dihedral angle being the most critical parameter. The influence of other geometric parameters, such as the CN bond length and the geometry of distant groups, is estimated to be of minor importance for the EPR parameters.

The direct influence of the surrounding amino acids on the EPR parameters of the spin label is found to be nonadditive; i.e., the total effect cannot be estimated as the sum of the changes due to the individual amino acids. This implies charge and/or spin density reorganization when increasing the model size.[38] Consequently, the calculated results can be sensitive to model construction. Granting the predominant role of the direct environmental effects due to the environmentally induced structure changes of the spin label, the problem may be of minor importance, however. Among the direct environmental effects, the change of the **g** tensor of the spin label itself completely dominates over the contributions from the surrounding amino acids.

Qualitative agreement with the experimental **g** tensor and dipolar part of the hyperfine coupling tensor is reached with the largest of the present models for the protein environment. A large error is observed for the isotropic hyperfine coupling constant, presumably due to deficiencies in the pure DFT exchange-correlation functionals employed.

In this study, the largest molecular model for the EPR parameters consists of a pyrrolidine nitroxide radical and five amino acids. Along with refs 38 and 39 the present study concerns the largest systems for which DFT calculations of EPR **g** tensors have been carried out. This implies the possibility to continue with calculations on spin labels at different positions in proteins. The combination of EPR spectroscopy and DFT calculations provides a prospect of obtaining detailed knowledge about the interaction between spin labels and other radicals in proteins. The possibility of making predictions of relations

between the EPR properties and geometric structure of radical sites is also indicated.

Acknowledgment. We are thankful to Ole H. Olsen at Novo Nordisk, Copenhagen, for giving us the coordinates of the MM calculations of MTSSL in the sTF/FVIIa complex. M.E. acknowledges Rikard Owenius for valuable discussions concerning the EPR spectroscopy of the sTF/FVIIa complex. J.V. thanks Marja Hyvönen, Martin Kaupp, and Henrik Konschin for critically reading the manuscript. The unknown referees are thanked for very useful suggestions. J.V. is on leave from the NMR Research Group, Department of Physical Sciences, University of Oulu, Finland, and has been supported by The Academy of Finland (grant 48578), and the Magnus Ehrnrooth Fund of the Finnish Society of Sciences and Letters. Computer time was supported by the National Supercomputer Center (NSC), the Center for Parallel Computers (PDC), and Center for Scientific Computing (CSC).

References and Notes

(1) Berliner, L. J.; Reuben, J. *Biological Magnetic Resonance*; Spin Labeling − Theory and Applications; Plenum Press: New York, 1989; Vol. 8.

(2) Hubbell, W. L.; Gross, A.; Langen, R.; Lietzov, M. A. *Curr. Opin. Struct. Biol.* **1998**, *8*, 649.

(3) Svensson, M.; Jonasson, P.; Freskgård, P.-O.; Jonsson, B. H., Lindgren, M.; Mårtensson, L.-G.; Gentile, M.; Borén, K.; Carlsson, U. *Biochemistry* **1995**, *34*, 8606.

(4) Lindgren, M.; Svensson, M.; Freskgård, P.-O.; Carlsson, U.; Jonasson, P.; Mårtensson, L.-G.; Jonsson, B. H. *Biophys. J.* **1995**, *69*, 202.

(5) Persson, M.; Hammarström, P.; Lindgren, M.; Jonsson, B. H.; Svensson, M.; Carlsson, U. *Biochemistry* **1999**, *38*, 432.

(6) Owenius, R.; Österlund, M.; Lindgren, M.; Svensson, M.; Olsen, O.-H.; Persson, E.; Freskgård, P.-O.; Carlsson, U. *Biophys. J.* **1999**, *77*, 2237.

(7) Kawamura, T.; Matsunami, S.; Yonezawa, T. *Bull. Chem. Soc. Jpn.* **1967**, *40*, 1111.

(8) Griffith, O.-H.; Dehlinger, P. J.; Van, S. P. *J. Membr. Biol.* **1974**, *15*, 159.

(9) Krinichnyi, V. I.; Grinberg, O. Ya.; Bogatyrenko, V. R.; Likhtenshtein, G. I.; Lebedev, Ya. S. *Biophysics* **1985**, *30*, 233.

(10) Ondar, M. A.; Grinberg, O. Ya.; Dubinskii, A. A.; Lebedev, Ya. S. *Sov. J. Chem. Phys.* **1985**, *3*, 781.

(11) Krinichnyi, V. I.; Grinberg, O. Ya.; Yudanova, Ye. I.; Lyubashevskaya, Ye. V.; Antsiferova, L. I.; Likhtenshtein, G. I.; Lebedev, Ya. S. *Biophysics* **1987**, *32*, 229.

(12) Ondar, M. A.; Grinberg, O. Ya.; Dubinskii, A. A.; Shestakov, A. F.; Lebedev, Ya. S. *Sov. J. Chem. Phys.* **1985**, *2*, 83.

(13) Mustafaev, S. A.; Schastnev, P. V. *J. Struct. Chem.* **1989**, *30*, 582.

(14) Earle, K. A.; Moscicki, J. K.; Ge, M.; Budil, D. E.; Freed, J. H. *Biophys. J.* **1994**, *66*, 1213.

(15) Steinhoff, H. J.; Savitsky, A.; Wegener, C.; Pfeiffer, M.; Plato, M.; Möbius, K. *Biochim. Biophys. Acta* **2000**, *1457*, 253.

(16) Steinhoff, H. J.; Pfeiffer, M.; Rink, T.; Burlon, O.; Kurz, M.; Riesle, J.; Heuberger, E.; Gerwert, K.; Oesterhelt, D. *Biophys. J.* **1999**, *76*, 2702.

(17) Narayan, M.; Berliner, L. J. *Protein Sci.* **1998**, *7*, 150.

(18) Biswas, R.; Kühne, H.; Brudvig, G. W.; Gopalan, V. *Sci. Prog.* **2001**, *84*, 45.

(19) Owenius, R.; Engström, M.; Lindgren, M. *J. Phys. Chem. A* **2001**, *105*, 10967.

(20) Miertus, S.; Scrocco, E.; Tomasi, J. *Chem. Phys.* **1981**, *55*, 117.

(21) Harlos, K.; Martin, D. M. A.; O'Brien, D. P.; Jones, E. Y.; Stuart, D. I.; Polikarpov, I.; Miller, A.; Tuddenham, E. G. D.; Boys, C. W. G. *Nature* **1994**, *370*, 662.

(22) Muller, Y. A.; Ultsch, M. H.; Kelley, R. F.; d. Vos, A. M. *Biochemistry* **1994**, *33*, 10864.

(23) Banner, D. W.; D'Arcy, A.; Chène, C.; Winkler, F. K.; Guha, A.; Konigsberg, W. H.; Nemerson, Y.; Kirchhofer, D. *Nature* **1996**, *380*, 41.

(24) Becke, A. D. *Phys. Rev. A* **1988**, *38*, 3098.

(25) Lee, C.; Yang, W.; Parr, R. G. *Phys. Rev. B* **1988**, *37*, 785.

(26) Dunning, T. H. Jr.; Hay, P. J. *Modern Theoretical Chemistry*; Plenum: New York, 1976.

(27) Frisch, M. J.; Trucks, G. W.; Schlegel, H. B.; Scuseria, G. E.; Robb, M. A.; Cheeseman, J. R.; Zakrzewski, V. G.; Montgomery, J. A., Jr.; Stratmann, R. E.; Burant, J. C.; Dapprich, S.; Millam, J. M.; Daniels, A. D.; Kudin, K. N.; Strain, M. C.; Farkas, O.; Tomasi, J.; Barone, V.; Cossi, M.; Cammi, R.; Mennucci, B.; Pomelli, C.; Adamo, C.; Clifford, S.; Ochterski, J.; Petersson, G. A.; Ayala, P. Y.; Cui, Q.; Morokuma, K.; Malick, D. K.; Rabuck, A. D.; Raghavachari, K.; Foresman, J. B.; Cioslowski, J.; Ortiz, J. V.; Baboul, A. G.; Stefanov, B. B.; Liu, G.; Liashenko, A.; Piskorz, P.; Komaromi, I.; Gomperts, R.; Martin, R. L.; Fox, D. J.; Keith, T.; Al-Laham, M. A.; Peng, C. Y.; Nanayakkara, A.; Challacombe, M.; Gill, P. M. W.; Johnson, B.; Chen, W.; Wong, M. W.; Andres, J. L.; Gonzalez, C.; Head-Gordon, M.; Replogle, E. S.; Pople, J. A. *Gaussian 98*, revision A.9; Gaussian, Inc.: Pittsburgh, PA, 1998.

(28) Perdew, J. P. *Phys. Rev. B* **1986**, *33*, 8822.

(29) Perdew, J. P.; Wang, Y. *Phys. Rev. B* **1986**, *33*, 8800.

(30) Malkin, V. G.; Malkina, O. L.; Eriksson, L. A,; Salahub, D. R. In *Modern density functional theory: A tool for chemistry*. Seminario, J. M., Politzer, P., Eds.; Theoretical and Computational Chemistry; Elsevier: Amsterdam, 1995; Vol. 2, p 273.

(31) Salahub, D. R.; Fournier, R.; Mlynarski, P.; Papai, I.; St-Amant, A.; Ushio, J. *Density functional methods in chemistry*; Springer: New York, 1991.

(32) St-Amant, A.; Salahub, D. R. *Chem. Phys. Lett.* **1990**, *169*, 387.

(33) Malkina, O. L.; Vaara, J.; Schimmelpfennig, B.; Munzarová, M.; Malkin, V. G.; Kaupp, M. *J. Am. Chem. Soc.* **2000**, *122*, 9206.

(34) Huzinaga, S. *Approximate Atomic Functions*; University of Alberta: Alberta, Canada, 1971.

(35) Kutzelnigg, W.; Fleischer, U.; Schindler, M. *NMR − Basic Principles and Progress*; Springer-Verlag: Heidelberg, 1990; Vol. 23.

(36) Chesnut, D. B.; Moore, K. D. *J. Comput. Chem.* **1985**, *10*, 648.

(37) Chesnut, D. B.; Rusiloski, B. E.; Moore, K. D.; Egolf, D. A. *J. Comput. Chem.* **1993**, *14*, 1364.

(38) Kaupp, M.; Remenyi, C.; Vaara, J.; Malkina, O. L.; Malkin, V. G. *J. Am. Chem. Soc.* **2002**, *124*, 2709.

(39) Kaupp, M. *Biochemistry* **2002**, *41*, 2895.

(40) Lushington, G. H.; Grein, F. *Theor. Chem. Acc.* **1996**, *93*, 1996.

(41) Pipek, J.; Mezey, P. G. *J. Chem. Phys.* **1989**, *90*, 4916.

(42) Hess, B. A.; Marian, C. M.; Wahlgren, U.; Gropen, O. *Chem. Phys. Lett.* **1996**, *251*, 365.

(43) Schimmelpfennig, B. *Atomic Spin−Orbit Mean-Field Integral Program*; Stockholms Universitet: Stockholm, 1996.

(44) Kaupp, M.; Reviakine, R.; Malkina, O. L.; Arbuznikov, A.; Schimmelpfennig, B.; Malkin, V. G. *J. Comput. Chem.* **2002**, *23*, 794.

(45) Malkin, V. G.; Malkina, O. L.; Casida, M. E.; Salahub, D. R. *J. Am. Chem. Soc.* **1994**, *116*, 5898.

(46) Eriksson, L. A.; Malkina, O. L.; Malkin, V. G.; Salahub, D. R. *J. Chem. Phys.* **1994**, *100*, 5066.

(47) Engström, M.; Owenius, R.; Vahtras, O. *Chem. Phys. Lett.* **2001**, *338*, 407.

(48) Suter, H. U.; Pless, V.; Ernzerhof, M.; Engels, B. *Chem. Phys. Lett.* **1994**, *230*, 398.

(49) Munzarová, M.; Kaupp, M. *J. Phys. Chem. A* **1999**, *103*, 9966.

(50) Barone, V. *J. Chem. Phys.* **1994**, *101*, 6834.